Ceramics-Silikáty 66 (4), 527-539 (2022)
www.ceramics-silikaty.cz doi: 10.13168/cs.2022.0049

INFLUENCE OF ALKALIS ON THE PHASE DEVELOPMENT OF BELITE-SULFOALUMINATE CLINKERS

BARBARA ČEPLAK*, KATARINA ŠTER**, MARUŠA MRAK**, LUKA ŠKRLEP**, MIRIJAM VRABEC***, #SABINA DOLENEC**

*Geological Survey of Slovenia, Dimičeva ulica 14, 1000 Ljubljana, Slovenia
**Slovenian National Building and Civil Engineering Institute, Dimičeva ulica 12, 1000 Ljubljana, Slovenia
***University of Ljubljana, Faculty of Natural Sciences and Engineering, Department of Geology Aškerčeva 12, 1000 Ljubljana, Slovenia

#E-mail: sabina.dolenec@zag.si

Submitted September 10, 2022; accepted October 10, 2022

Keywords: Belite-sulfoaluminate clinker, Clinker microstructure, Alkalis, Reactivity

This paper presents a study on the influence of different amounts of alkalis (K_2O and Na_2O) on clinker phase formation, microstructure, phase composition and reactivity of belite-sulfoaluminate cement clinker. Using X-ray powder diffraction and scanning electron microscopy with energy dispersive spectrometry, it was found that the amount of C_2S and C_4AF increases with the incorporation of alkalis, while the amount of $C_4A_3\bar{S}$ and $C\bar{S}$ decreases. In addition to the major phases, the samples with alkalis also consist of minor phases such as C_3A (tricalcium aluminate), $K\bar{S}$ (arcanite), and $KC_2\bar{S}_3$ (Ca-langbeinite). The major ions in the major phases were substituted by alkali cations and some other ions (Ca^{2+}, Al^{3+}, Fe^{3+}, S^{2-}, S^{6+}, Si^{4+}). The alkalis also affect the microstructure of the clinker, e.g., the shape of the grains. Consequently, isothermal calorimetry was used to detect differences in hydration kinetics. The clinker with 2 wt. % K_2O content was the most reactive, while the sample with 0.5 wt. % Na content was the least reactive. The latter was primarily influenced by the content of the main and minor phases of the clinker.

INTRODUCTION

The cement industry is one of the fastest growing industries. After fossil fuels and changes in land use, it is the third largest source of anthropogenic emissions of carbon dioxide (CO_2). This type of emission is estimated to account for 8 % of global anthropogenic CO_2 emissions [1]. Recently, several studies are striving to find a new type of binder that can provide lower CO_2 emissions [2, 3]. Belite sulfoaluminate cement (BCSA) is also one of these binders. Its lower embodied energy and CO_2 emissions compared to ordinary Portland cement (OPC) production are related to lower limestone requirement, lower grinding energy and lower sintering temperatures [2, 4].

BCSA cement clinker generally consists of the following phases: belite (Ca_2SiO_4 or C_2S in cement notation), calcium sulfoaluminate (Ca_2SiO_4 or $C_4A_3\bar{S}$), and ferrite ($Ca_2(Al,Fe)_2O_5$ or C_4AF), followed by calcium sulfate ($CaSO_4$ or $C\bar{S}$) [4]. In addition to major phases, BCSA clinkers also contain so-called minor components [5]. The most commonly reported are gehlenite ($Ca_2Al_2SiO_7$ or C_2AS), periclase (MgO or M), mayenite ($12CaO{\cdot}7Al_2O_3$ or $C_{12}A7$), perovskite ($CaTiO_4$ or CT), arcanite (K_2SO_4 or $K\bar{S}$), free lime (CaO or C), and magnetite (Fe_3O_4 or fF) [6, 7]. The formation of minor components strongly depends on the minor elements present in the raw mixture for clinker [8]. The presence of minor elements also affects among other things, the clinker microstructure [9]. The clinker microstructure is defined by the size and shape of the clinker grains [10] and is formed during the sintering of raw materials for clinker [11]. The development of clinker grains depends on the physicochemical properties of the liquid phase in the process of clinker formation. When the composition of the liquid changes, it affects the surface tension, viscosity, and temperature of the formation of the liquid phase, and finally on clinker microstructure [12].

Alkalis are the most abundant minor components in natural materials [13] and are inevitably introduced into cement clinker in small quantities because they are components of raw materials and fuel for clinker sintering [12]. The content of alkalis in raw meals is also increasing due to industrial by-products and/or wastes, which have increasingly replaced raw materials for clinker production in recent years [7, 14–16]. Alkalis affect the mineral composition, shape, and size of the phases [15, 17–19] and consequently the hydration rate [20]. Numerous papers addressed the effect of alkalis on the phase composition of Portland clinker and the

properties of Portland cement. The results show that the activation effect of K_2O and Na_2O is slightly different. Thus, clinkers with K_2O incorporation consisted of a higher amount of ά-C_2S than those with Na_2O incorporation, in which α-C_2S predominated [21]. Na_2O and K_2O are predominantly incorporated into aluminate (C_3A) in absence of SO_3 [18, 22], while these two alkalis are predominantly incorporated into belite (C_2S) in case of belite-rich OPC. In this case, the substitution for K_2O is higher than for Na_2O [23]. The results also illustrated the effect of alkalis on the stabilization of high-temperature belite modification (α and ά) [6, 18, 21, 23] and its effect on hydration kinetics. The incorporation of Na_2O into C_3A inhibits the hydration kinetics of OPC, while K_2O accelerates it [22].

To date, few studies have addressed the microstructure of BCSA clinkers [7, 24–28]. The results showed that the microstructure of BCSA clinker strongly depends on the phase composition [27]. In general, the microstructure is fine-grained with intermediate pores of different shapes and sizes while the grains of the clinker phases are randomly oriented and uniformly distributed throughout the sample [26]. Usually, the euhedral and subhedral calcium sulfoaluminate ($C_4A_3Ś$) grains are enclosed in an interstitial mixture formed consisting mainly of belite C_2S and ferrite (C_4AF) phases [29]. The cooling regime and sintering temperature play an important role when dealing with the microstructure of the BCSA clinker. The cooling regime regulates the size and morphology of the grains of the major phases [7], while the sintering temperature regulates the degree of crystallization [26]. The alkalis lower the sintering temperature of BCSA and consequently affect the clinker microstructure, phase development, size, and shape of phase grains [28]. The hydration kinetics of BCSA clinkers is influenced by both the major and minor phases [7]. In the case of alkali incorporation in alite-sulfoalumiante cement clinkers, the amount of $C_4A_3Ś$ is decreased [19], and in clinkers with a high amount of sulfoaluminate phase, the grains become rounded [24], while the size of the mostly rounded belite grains was reduced in belite-rich clinkers [17]. Potassium and sodium are most commonly incorporated into the crystal lattice of $C_4A_3Ś$, less so into the crystal lattice of C_2S and C_4AF [25].

Based on this study, the influence of the type and amount of alkalis on the formation of major and minor clinker phases, the possible incorporation of foreign ions into the major clinker phases, the effect of alkalis on the microstructure of the clinker, and the rate of clinker reactivity were studied. The cement clinker with the following phase composition: 60 wt. % C_2S, 20 wt. % $C_4A_3Ś$ (calcium sulfoaluminate), 10 wt. % C_4AF (ferrite) and 10 wt. % CŚ (anhydrite) was synthesized, containing two types of alkalis (K_2O and Na_2O) in three different proportions (0.5, 1 and 2 wt. %).

EXPERIMENTAL

Materials

The clinkers in the study were synthesized from pure chemicals. The reagent-grade chemicals used to produce BCSA cement clinker were calcium carbonate (purity of 99.0 %, Acros Organics), iron (III) oxide (purity of 95.0 %, Acros Organics), calcium sulphate-2-hydrate (purity of 99.9 %, Kemika d.d.), silicon dioxide (purity of 99.5 %, Sigma-Aldrich), aluminium oxide (purity of 99.7 %, Acros Organics), sodium carbonate (purity of 99.5 %, Kemika d.d.) and potassium carbonate (purity of 99.0 %, Alkaloid). The chemical composition of the clinker was calculated using the Bogue equation [30].

BCSA clinker (labelled Re) was prepared as a reference material. Its composition was as follows: 60 wt. % C_2S, 20 wt. % $C_4A_3Ś$, 10 wt. % C_4AF, and 10 wt. % CŚ [31]. Additionally, six BCSA clinkers were prepared with alkalis. K_2CO_3 (99.0 %, Alkaloid) was incorporated into the raw mixture to obtain theoretical nominal dosages of 0.5, 1 and 2 wt. % K_2O, hereafter referred to as 0.5K, 1K, 2K. Similarly, Na_2CO_3 (99.5 %, Kemika) was applied to obtain theoretical values of 0.5, 1 and 2 wt. % Na_2O, hereafter referred to as 0.5Na, 1Na and 2Na, respectively. Table 1 shows the chemical composition of the raw mixtures, expressed as oxides, required to produce clinkers.

Table 1. Chemical composition of the raw mixtures for synthesis of clinkers (wt. %).

Sample	CaO	SiO_2	Al_2O_3	Fe_2O_3	SO_3	K_2O	Na_2O
Re	55.15	20.93	12.12	3.29	8.51	0.00	0.00
K_2O (wt. %)							
0.5	54.89	20.82	12.06	3.27	8.46	0.50	0.00
1	54.61	20.72	12.00	3.25	8.42	1.00	0.00
2	54.05	20.51	11.88	3.22	8.34	2.00	0.00
Na_2O (wt. %)							
0.5	54.89	20.82	12.06	3.27	8.46	0.00	0.50
1	54.61	20.72	12.00	3.25	8.42	0.00	1.00
2	54.05	20.51	11.88	3.22	8.34	0.00	2.00

Legend. Re - reference sample, K-K_2O, Na-Na_2O, 0.5, 1, 2 – the alkali content added to the raw mixture (wt. %)

For the synthesis and analysis of cement clinker, 50 g of the raw mixture was prepared. The starting raw materials were dry homogenized using Turbula T2F homogenizer. The raw mixture was homogenized in the 0.25 l plastic box for one hour in the presence of two steel balls with a diameter of 1 cm. Subsequently, pressed pellets with a diameter of 3 cm were prepared from each homogenized mixture. Each pellet contained 15 g of the material. These pellets were pressed using an HPM 25/5 press at 10.6 kN and subsequently heated to 1300 °C in a Protherm PLF 160/9 furnace with a heating of 10 °C·min^{-1}, a residence time at maximum temperature of 1 h, and natural cooling in a closed furnace.

Methods

The phase composition of the clinkers was determined by X-ray powder diffraction analysis (XRD) using a PANalytical Empyrean X-ray diffractometer equipped with CuKα radiation with λ = 1.54 Å. Samples were ground to a particle size < 0.063 mm and manually loaded into a circular sample holder with a diameter of 10 mm. Samples were scanned at 40 mA and a voltage of 45 kV, over the 2θ range from 4° to 70°, with a step size of 0.026° 2θ and a scan step time of 197 s. PANalytical X`Pert Highscore Plus diffraction software v. 4.9 was used to the determination the phase composition, using PAN ICSD v. 3.4 powder diffraction files. The powder diffraction file codes (PDF) for the identified phases used for the Rietveld refinements were as follows: β-C_2S (00-033-0302), $C_4A_3Ś$-orthorhombic (01-083-9042), $C_4A_3Ś$-cubic (01-083-7086), C_4AF (98-009-8836), CŚ (00-037-1496), calcium aluminate – C_3A-cubic (00-038-1429), C_3A-orthorhombic (01-070-0859), arcanite – KŚ (00-005-0613) and Ca-langbeinite – $KC_2Ś_3$ (00-020-0867).

In order to determine the possible changes in the lattice parameters as a consequence of the incorporation (e.g., substitution) of the foreign ions into the structure of the major phases, the shift of the XRD peaks in the alkali-incorporated samples was analysed in comparison with the reference sample. For this purpose, the interplanar distances between the atoms in the crystals of the three main clinker phases – d-values (C_2S, $C_4A_3Ś$ and C_4AF) – were studied. The distinct peaks of the powder diffraction pattern for C_2S are 2.783 Å (100 %) 2.790 Å (97 %), and 2.610 Å (42 %), for $C_4A_3Ś$ are 3.760 Å (100 %), 2.656 Å (36 %) and 2.172 Å (24 %), and for C_4AF are 2.638 Å (100 %), 1.924 Å (46 %) and 7.248 Å (32 %).

The clinker microstructure was observed on polished cross-sections examined by using JEOL JSM-IT500 LV Scanning Electron Microscope (SEM) equipped with an Energy Dispersive X-ray spectrometer (EDS) (Oxford Instruments). Images were taken at a working distance of 20 mm and 10 mm, respectively, and an accelerating voltage of 20 kV. The SEM/EDS method was used to observe the microstructure of clinker, while EDS was used to determine the chemical composition of the clinker and the elemental distribution.

The reactivity of the clinker was studied by isothermal calorimetry, using TAM Air 8 (TA instruments). For the analysis, a pellet of clinker was crushed in a mortar and sieved to a size below 125 μm. Subsequently, 4 g of each sample was used at a water/cement ratio of 0.5, stirred for 3 minutes and placed in glass containers. Heat evolution was measured at 20 °C for 7 days.

Table 2. Phase composition of synthesized clinkers as determined by Rietveld refinement (wt. %).

		K_2O (wt. %)			Na_2O (wt. %)		
Phase	Re	0.5	1	2	0.5	1	2
β-C_2S	64.6	71.9	70.6	71.8	68.6	71.7	75.5
o-$C_4A_3Ś$	22.8	14.0	14.4	10.0	16.2	13.7	5.5
c-$C_4A_3Ś$	2.2	2.7	1.5	n.d.	3.7	0.7	1.9
Σ $C_4A_3Ś$	25.0	16.7	15.9	10.0	19.9	14.4	7.4
C_4AF	5.2	6.6	7.1	8.0	7.1	8.6	9.1
CŚ	5.2	3.3	2.2	0.1	4.4	3.8	2.6
o-C_3A	n.d.	n.d.	n.d.	0.2	n.d.	n.d.	0.6
c-C_3A	n.d.	n.d.	0.9	5.2	n.d.	1.5	4.8
Σ C_3A	n.d.	n.d.	0.9	5.4	n.d.	1.5	5.4
KŚ	n.d.	0.2	0.5	0.5	n.d.	n.d.	n.d.
$KC_2Ś_3$	n.d.	1.3	2.8	4.2	n.d.	n.d.	n.d.

Legend. n.d. – not determined

RESULTS AND DISCUSSION

X-ray powder diffraction

The phase composition of cement clinker, determined by Rietveld refinement, is shown in Table 2. The XRD patterns of selected samples are shown in Figure 1. In addition to the presence of major phases in clinkers, such as belite (C_2S), calcium sulfoaluminate ($C_4A_3Ś$), ferrite (C_4AF) and anhydrite (CŚ), minor phases were also present (tricalcium aluminate (C_3A), arcanite (KŚ), and Ca-langbeinite ($KC_2Ś_3$)). While in the reference sample the overall content of the major clinker phases was close to the target values, differences in the phase composition were detected in alkali containing samples.

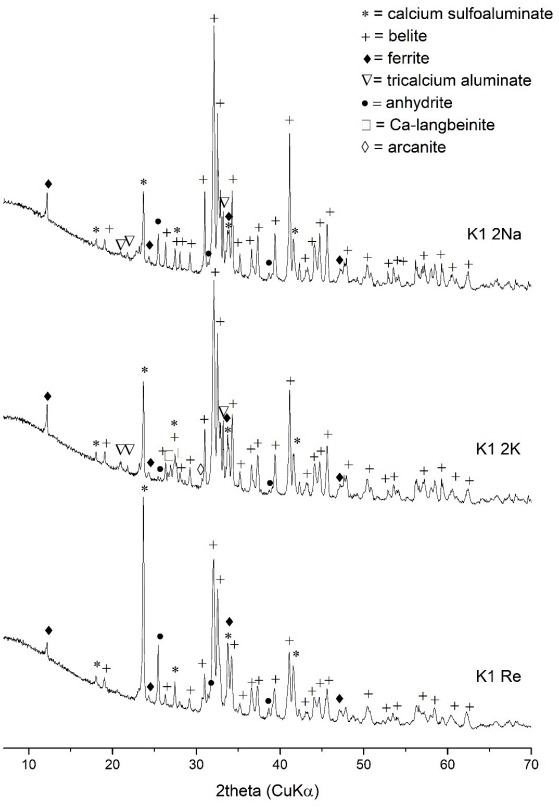

Figure 1. X-ray powder diffraction patterns of selected samples (Re, 2K and 2Na).

The addition of alkalis in different proportions (0.5, 1 or 2 wt. %) affects the phase composition of clinker. The amount of C_2S does not change significantly with increasing amount of incorporated K_2O, however, the quantities in all three samples are higher than in the reference sample. The amount of C_2S increases linearly with the Na_2O content (Figure 2). In general, a higher amount of C_2S was identified in the samples containing Na_2O, while the reference sample had the lowest C_2S content. These changes can be related to the charge and size of the substituted cations or anions. For example, Na^+ and K^+, which are larger than Ca^{2+}, can substitute Ca^{2+}, increasing the belite content [32]. Increasing the content of alkalis induced stabilization of β-C_2S. Foreign ions incorporated into the C_2S crystal lattice can increase or decrease the final amount of C_2S [32] and stabilize the C_2S polymorphs. Namely, the cations larger than Ca^{2+} (e.g., Na^+ and K^+) increase the volume of the cells [21] and in this way stabilize the β-C_2S [33]. On the other hand, the stabilization of the C_2S polymorph may also be related to the polarization ability of the ions. Xiuji and Shizong [34] found that ions having either lower polarizability than the Ca^{2+} ion or higher polarizability than the Si^{4+} ion can affect the stability of β-C_2S.

As can be seen in Figure 2, the amount of $C_4A_3\acute{S}$ decreased with alkali content which is opposite to the C_2S trend. Alkalis can affect the physicochemical properties of the melt and the phase composition of the clinker [12] and consequently affect the crystallization pathways of $C_4A_3\acute{S}$ and C_2S formation. However, in this study, the amounts of C_2S and $C_4A_3\acute{S}$ increase and decrease, respectively, only in samples with Na_2O, which may be related to the formation of alkali sulfates in samples with K_2O admixture. There, the amount of $C_4A_3\acute{S}$ decreases because SO_3^{2-} is used to form alkali sulfate and not as a replacement ion in the C_2S lattice as in samples with Na_2O addition. In the alkali incorporated samples, regardless of the type of alkali, $C_3A_4\acute{S}$ never reached the target value, which could be due to the formation of alkali sulfates or to the partial volatilization of sulfur from unreacted anhydrite or its partial decomposition in C_3A and the release of SO_2 [35] (Table 2). In general, the decrease of the calcium sulfoaluminate phase is higher in Na_2O-incorporated clinkers due to the formation of haüyn, the endmember of the sodalite solid solution, where Ca^{2+} and Al^{3+} are replaced by Na^+ and Si^{4+} [36]. The highest $C_4A_3\acute{S}$ amount is therefore characteristic of the reference sample. The dominant polymorph of $C_4A_3\acute{S}$ in all seven clinkers was orthorhombic. With respect to the reference sample, the decrease in orthorhombic polymorphs is evident with the addition of both alkalis, especially significant at the highest alkali contents. In addition to the effects of the alkalis on the stabilization of the C_2S polymorph, the effect of the alkalis on the stabilization of $C_4A_3\acute{S}$ was also demonstrated. The crystal lattice of $C_4A_3\acute{S}$ at room temperature was reported to be tetragonal, cubic, and orthorhombic [36]. Moreover, the C_4AF content increased with an increasing amount of alkalis, which was previously found in a study by Žibret et al. [28]. Slightly higher effects were found for Na_2O-incorporated clinkers. The content of $C\acute{S}$ also decreases proportionally with a higher amount of alkalis, which means that the highest amount is characteristic for the reference sample. Higher concentrations were found in samples with Na_2O, which may be related to the absence of alkali sulfates in these samples.

Among the minor phases, C_3A, $C\acute{S}$, $K\acute{S}$, and $KC_2\acute{S}_3$ were detected. The C_3A was present in orthorhombic and cubic forms. The orthorhombic C_3A was identified in samples containing 2 wt. % of K_2O and N_2O, while cubic C_3A was detected in samples with 1 and 2 wt. % of K_2O and Na_2O, respectively. Moreover, $K\acute{S}$ and $KC_2\acute{S}_3$ were identified in all three samples with K_2O, and the amount of $KC_2\acute{S}_3$ increased with the higher amount of alkalis (Table 2, Figure 1).

The amount of $C_4A_3\acute{S}$ is dependent on the amount of SO_3 [19]. Namely, due to the high amount of Na_2O and K_2O, alkali sulfates begin to form, leading to a decrease in the amount of SO_3 available for $C_4A_3\acute{S}$ formation [12, 19]. This phenomenon is observed in

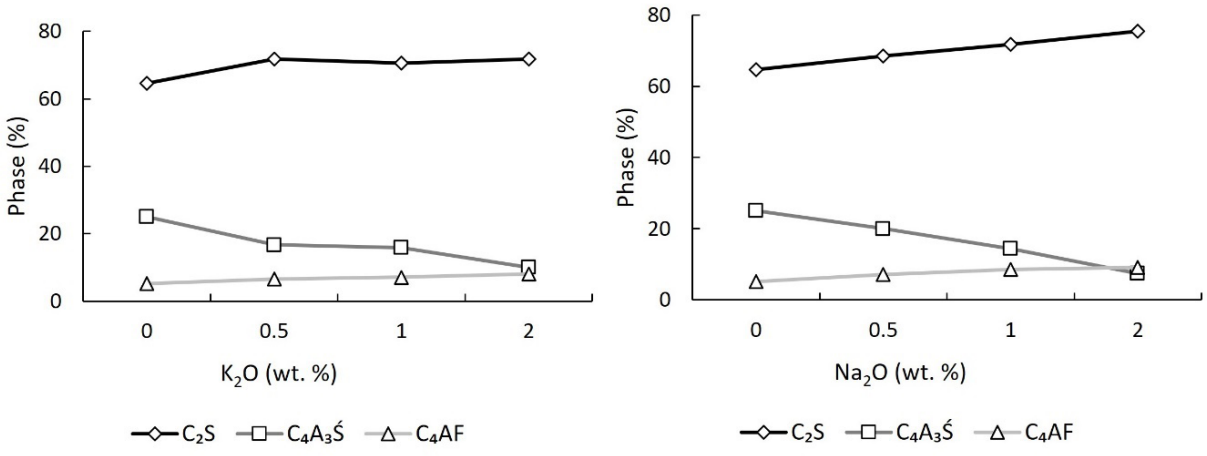

Figure 2. Amount of major phases in reference clinker and clinkers with different proportions of Na_2O and K_2O.

the samples with the incorporation of K_2O. KŚ and $K_2CŚ_3$ were determined in these samples. In the case of Na_2O samples, a small amount of $C_4A_3Ś$ may be a consequence of the decomposition of this phase starting at 1300 °C [27] or a result of the formation of haüyn [36]. The high amount of C_4AF in samples with a higher amount of alkalis is connected to the lowering of the melting point of C_4AF in the presence of alkalis [24]. The small amount of CŚ in samples with K_2O may be a consequence of the formation of KŚ and $KC_2Ś_3$ [19], consuming SO_3. For the samples that contained a larger amount of alkalis, the small amount of CŚ could also be related to the decomposition of CŚ and the presence of C_3A. The decomposition of CŚ causes the evaporation of sulfur and the formation of CaO [24]. The free CaO then reacts with Al_2O_3, leading to the decomposition of $C_4A_3Ś$, forming C_3A [5].

The incorporation of foreign ions into the crystal lattices of the major phases can be further confirmed by the shift of the peaks of the major phases (Table 3). The structure of C_2S, $C_4A_3Ś$ and C_4AF allows the incorporation of other atoms into the structure, resulting in variable d-values. C_2S can substitute the Ca^{2+} sites with other anions and cations, such as Na^+, K^+ or S^{2-}, or Si^{4+} for Fe^{3+} and Al^{3+} [20]. In $C_4A_3Ś$, Na^+ and K^+ cations can replace Ca^{2+} ions, while Al^{3+} is replaced by Si^{4+} and Fe^{3+} [4, 33]. In C_4AF, Al^{3+} and Fe^{3+} ions are mostly replaced by Si^{4+} and S^{6+} ions [26], while Ca^{2+} is substituted by monovalent bivalent ions, such as alkalis [24]. The changes in d-values are strongly related to ionic radii, i.e., smaller ionic radii of the replacement ions decrease cell parameters and vice versa [37].

The d-values of the C_2S, $C_4A_3Ś$, and C_4AF peaks were generally lower in the samples with higher K_2O or Na_2O content than in the samples with lower alkali content or in the reference samples. It is therefore evident that the d-spacing changes with the addition of alkalis and other foreign ions, suggesting that ions with smaller ionic radii (e.g., S^{6+}) are incorporated into the C_2S, $C_4A_3Ś$, and C_4AF crystal lattices, where they replace ions with larger ionic radii (e.g., Ca^{2+}). However, there are some differences, especially in the $C_4A_3Ś$ crystal lattice of the samples with the incorporation of K_2O, where the d-values are higher in the samples with a higher amount of alkalis, indicating the incorporation of ions with larger ionic radii (e.g., K^+) into the $C_4A_3Ś$ crystal lattice and their substitution by ions with smaller radii (e.g., Ca^{2+}). However, it should be noted that the ionic radii of some original and substituted ions are similar, so their presence or absence cannot be confirmed by observation of d values alone (e.g., Na^+ - 116 pm, Ca^{2+} - 114 pm).

SEM/EDS

Clinker microstructure

The influence of different amounts and types of alkalis on the development of microstructure and phase composition was further studied using SEM/EDS. The clinker samples showed a holocrystalline microtexture; the grains are evenly distributed throughout the sample (Figure 3). In all samples, C_2S and $C_4A_3Ś$ were the dominant phases, with the C_4AF phase appearing as euhedral and anhedral grains. The sample also consisted of the CŚ phase and other minor components, e.g., C_3A, KŚ, and $K_2CŚ_4$, which mainly formed an interstitial phase. All samples consisted of $C_4A_3Ś$ agglomerates in which anhedral C_2S and C_4AF grains appeared. Around these agglomerates, mainly C_2S phase with hardly recognisable boundaries occurs in samples with incorporated alkalis (Figure 3).

In the reference sample, the C_2S phase was mainly represented by rounded C_2S grains which were mostly spherical and ranged in size from 1.2 to 29.7 μm, including often interstitial CŚ (Figure 4). $C_4A_3Ś$ phases mostly occurred in clusters, but also as an interstitial phase among C_2S. In most cases, the single $C_4A_3Ś$ phase was very well differentiated and exhibited euhedral six-sided crystal grains ranging in size from 0.9 to 12.2 μm. Among the clusters formed by $C_4A_3Ś$ grains, anhedral C_2S and C_4AF occurred. The C_4AF phase occurs as an interstitial phase, but the majority of the phase is seen as acicular euhedral grains ranging in size from 3 to 22.5 μm. In some places, C_4AF laths surrounded clusters of $C_4A_3Ś$ grains, indicating the subsequent formation of C_4AF with respect to $C_4A_3Ś$ (Figure 4) [27].

Clinker samples with the addition of K_2O generally consisted of the C_2S phase, in which hardly any grain

Table 3. D-values of selected peaks for C_2S, $C_4A_3Ś$ and C_4AF phases (in Å).

	Sample	C_2S			$C_4A_3Ś$			C_4AF		
	Re.	2.783	2.790	2.610	3.760	2.656	2.172	2.638	1.924	7.248
		(100%)	(97%)	(42%)	(100%)	(36%)	(24%)	(100%)	(46%)	(32%)
K content	0.5	2.788	2.801	2.619	3.761	2.656	2.172	2.649	1.931	7.276
(wt. %)	1	2.789	2.801	2.619	3.761	2.657	2.173	2.644	1.928	7.270
	2	2.787	2.800	2.617	3.760	2.657	2.172	2.642	1.927	7.264
Na content	0.5	2.788	2.800	2.620	3.761	2.657	2.173	2.656	1.931	7.274
(wt. %)	1	2.788	2.800	2.620	3.760	2.656	2.172	2.646	1.929	7.270
	2	2.787	2.799	2.617	3.760	2.656	2.171	2.642	1.926	7.265

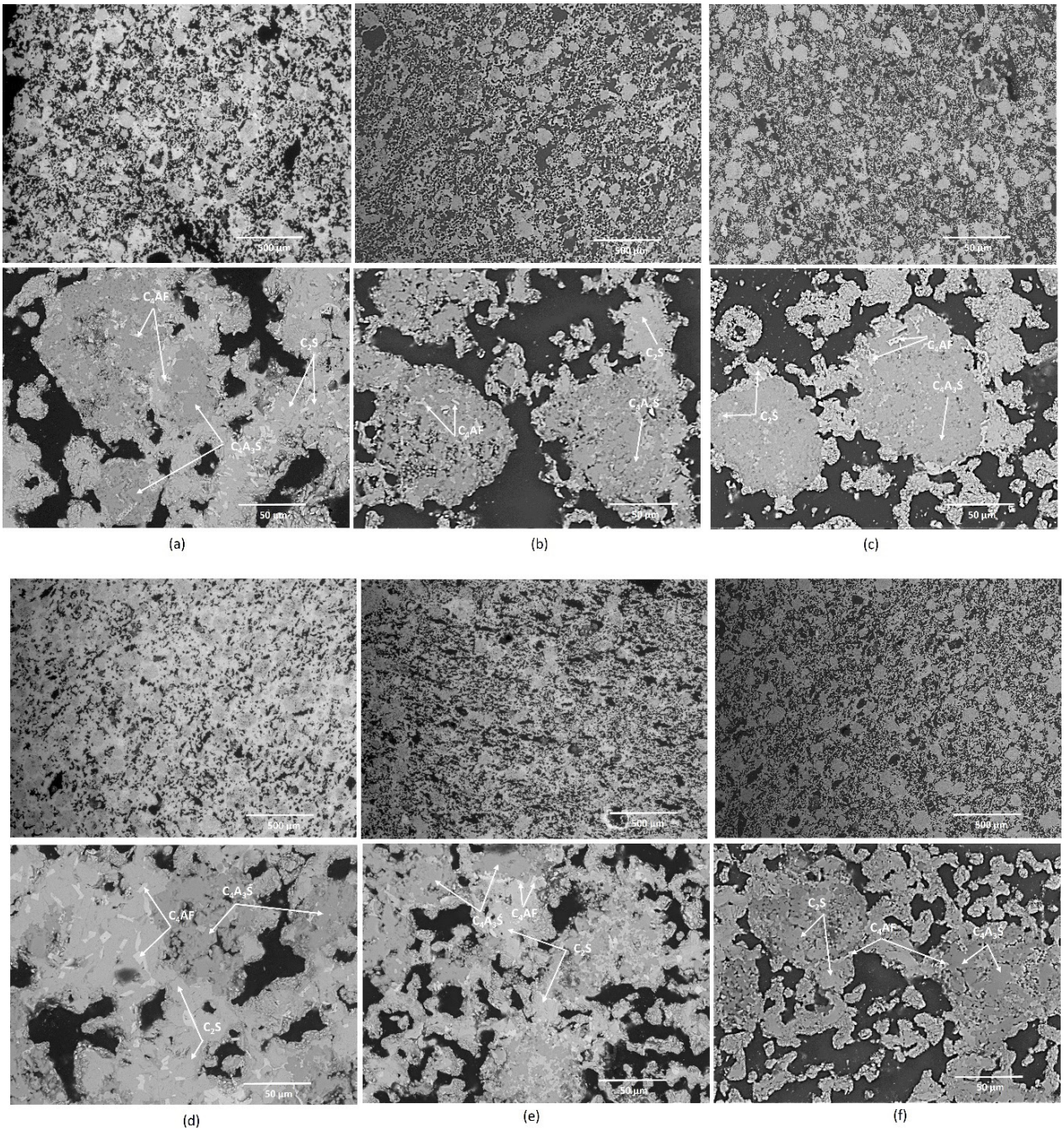

Figure 3. The phase composition of clinkers: a) 0.5K, b) 1K, c) 2K, d) 0.5Na, e) 1Na, f) 2Na, at different magnifications (Scanning Electron Microscope (SEM)/Backscattered Electron (BSE) micro-photographs).
Clinker phase designations: C_2S = belite, $C_4A_3\acute{S}$ = calcium sulfoaluminate and C_4AF = ferrite.

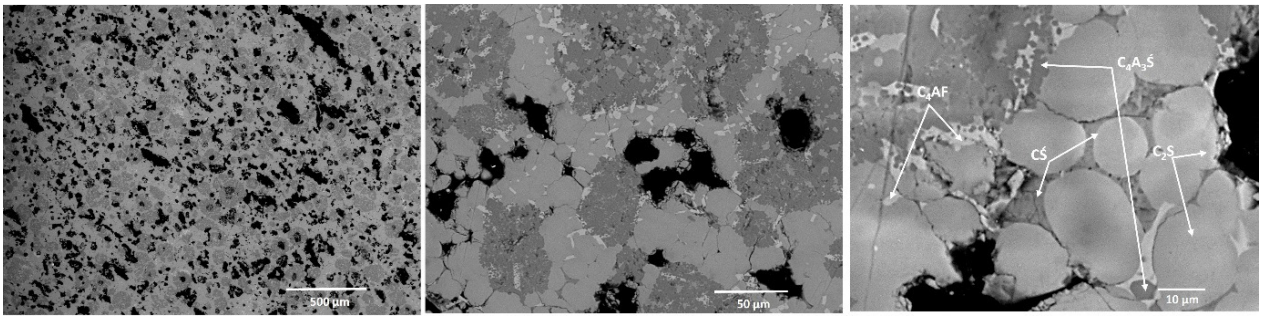

Figure 4. The SEM/BSE phase composition of reference sample at different magnifications.
Clinker phase designations: C_2S = belite, $C_4A_3\acute{S}$ = calcium sulfoaluminate, C_4AF = ferrite and $C\acute{S}$ = anhydrite

boundaries could be seen. In the samples with 0.5 and 2 wt. % K_2O, where this was possible, the C_2S grains were mostly irregularly shaped (Figures 5a and 5c), while the sample with 1 wt. % K_2O consisted mainly of spherical and elongated C_2S grains (Figure 5b). The size of the grains ranged from 2 to 12.8 μm, 2.8 to 18.3 μm, and 1.6 to 13.3 μm for 0.5K, 1K, and 2K, respectively. The $C_4A_3Ś$ phase was mostly identified in the clusters in all three samples, while individual grains in 0.5K appeared like euhedral, rarely like subhedral grains (Figure 5a) but subhedral grains predominated in the samples with 1 and 2 wt. % K_2O (Figures 5b and 5c). In 0.5K, these grains are mostly hexagonal, while in the samples with higher alkali content, grains with more rounded edges appeared. In the 2K, the grains became spherical. The size ranged from 1 to 8.3 μm for 0.5K, from 1.7 to 11 μm for 1K, and

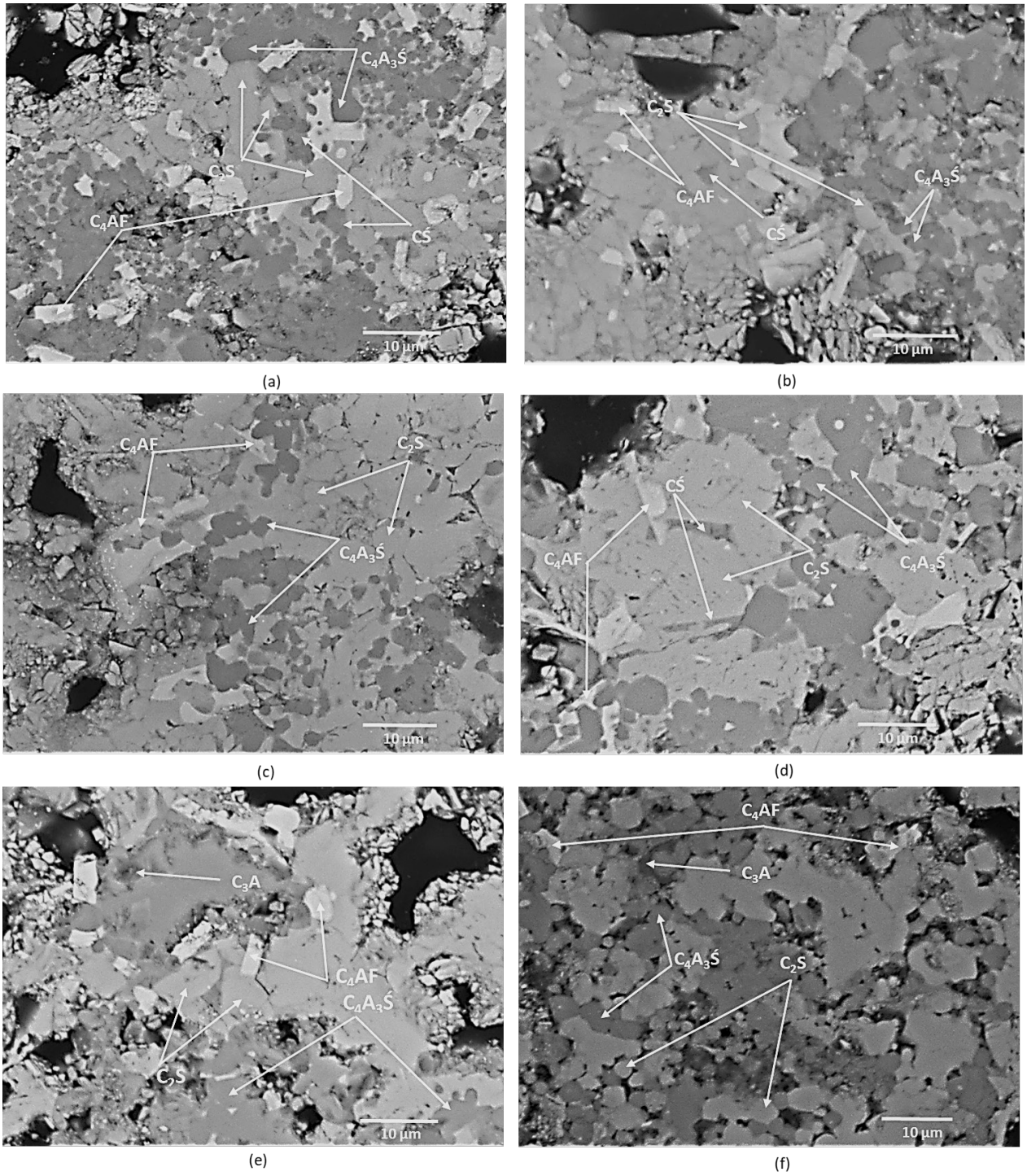

Figure 5. Microstructure of samples with the incorporation of alkalis: a) 0.5K, b) 1K, c) 2K, d) 0.5Na, e) 1Na and f) 2Na. Clinker phase designations: C_2S = belite, $C_4A_3Ś$ = calcium sulfoaluminate, C_4AF = ferrite and $CŚ$ = anhydrite.

from 3 to 13.4 µm for 2K. The majority of the C_4AF phase characteristic for 0.5K appeared as euhedral, acicular grains ranging from 2.3 to 10.4 µm (Figure 5a), while the grains in 1K and 2K exhibit subhedral, mostly irregularly shaped (Figures 5b and 5c). The size of the grains ranged from 2.3 to 10.4 µm, 1.5 to 14.9 µm, and 1.7 and 7.9 µm for 0.5K, 1K, and 2K, respectively. In all three samples, the C_2S grains were frequently surrounded by calcium sulfoaluminate grains. Furthermore, the occurrence of CŚ, KŚ, and $K_2CŚ_4$ mainly as an interstitial phase, was observed in all three samples.

Clinker samples with incorporated Na_2O generally consist of subhedral C_2S, irregularly shaped or spherical grains ranging in size from 2.9 to 25.7 µm for 0.5Na (Figure 5d), from 1.7 to 20.1 µm for 1K (Figure 5e), and from 2.1 to 10.4 µm for 2Na (Figure 5f). The $C_4A_3Ś$ phase appears in the sample with 0.5 wt. % Na as subhedral, irregularly shaped grains and also as euhedral, six-sided grains ranging between 0.8 and 14.6 µm (Figure 5d). In samples containing 1 and 2 wt. % Na_2O, subhedral grains predominate, being either spherical or irregularly shaped and ranging in size from 0.8 to 10.4 µm for 1Na (Figure 5e) and from 1.6 to 12.1 µm for 2Na (Figure 5f). The C_4AF phase in 0.5Na and 1Na consists mainly of euhedral and acicular in shape but also as subhedral and anhedral grains (Figures 5d and 5e), while subhedral tabular and irregularly shaped grains predominate in 2Na (Figure 5f). The size of the ferrite grains ranged from 1.8 to 24.6 µm, 1.1 to 6.2 µm, and 1.1 to 6.2 µm for 0.5Na, 1Na, and 2Na, respectively. In all three samples, CŚ occurred as part of the interstitial phase. In addition to the clinker phase mentioned above, the presence of C_3A was also identified in 1Na and 2Na (Figures 5e and 5f).

The presence of alkalis strongly affects the shape of major phases' grains. The C_2S grains are generally spherical in the reference sample, while subhedral and anhedral grains predominate in the samples with alkali incorporation (Na_2O and K_2O). Thus, as noted in the study by Saidani et al. [38], the addition of foreign ions affected the morphology of the C_2S grains. Focusing on $C_4A_3Ś$ grains, euhedral shapes predominate in the reference sample, while hexagonal shapes predominate in the samples with a low content of both types of alkalis, indicating well-crystallized grains [26, 31]. In samples with a higher content of alkalis (Na_2O and K_2O), subhedral and spherical grains occur. In the reference sample and samples with a lower content of both types of alkalis, the C_4AF grains are euhedral, mostly long prismatic. As the alkali content increases, they become more subhedral. It was found that a small quantity of Fe^{3+} in the C_4AF solid solution, leads to the formation of long-prismatic grains, while a higher quantity of Fe^{3+} ions in the C_4AF results in the subhedral C_4AF grains [27].

Chemical composition of clinker phases

EDS analyses of the three major phases in clinkers showed that C_2S contains Al^{3+}, S^{2-}, Fe^{3+}, Na^+, and K^+ in addition to Ca^{2+} and Si^{4+}. The $C_4A_3Ś$ grains consist of Ca^{2+}, Al^{3+}, and S^{2-} and also have some Na^+, K^+, Si^{4+}, and Fe^{3+}. The following ions were determined in the C_4AF grains: Ca^{2+}, Al^{3+}, Fe^{3+}, Si^{4+}, S^{2-}, Na^+, and K^+, which is also shown in Figure 6 for the sample with 0.5 wt. % Na_2O. All substitutions found in the clinker phases are consistent with previous studies [20, 24, 26] and have already been observed as changes in the d-values of the major phases (Table 3). In order to improve the observations, an additional analysis was performed.

Ca^{2+} ions in the crystal lattice of C_2S, $C_4A_3Ś$, and C_4AF are substituted by K^+ and Na^+ (Figure 7). The ratio of Na/Ca and K/Ca increases proportionally to higher alkali content (Figure 7a). K^+ ions are incorporated into the crystal lattice to a greater extent than Na^+ ions, which was noted in the earlier study by Gies and Knöfel [23]. In general, Na^+ ions are preferably incorporated into the $C_4A_3Ś$ crystal lattice forming haüyn [36].

Moreover, Si^{4+} ions in C_2S are substituted by Fe^{3+}, Al^{3+}, and S^{6+} (Figures 7b, 7c and 7d), which is consistent with an earlier study [39]. The substitution of Si^{4+} with

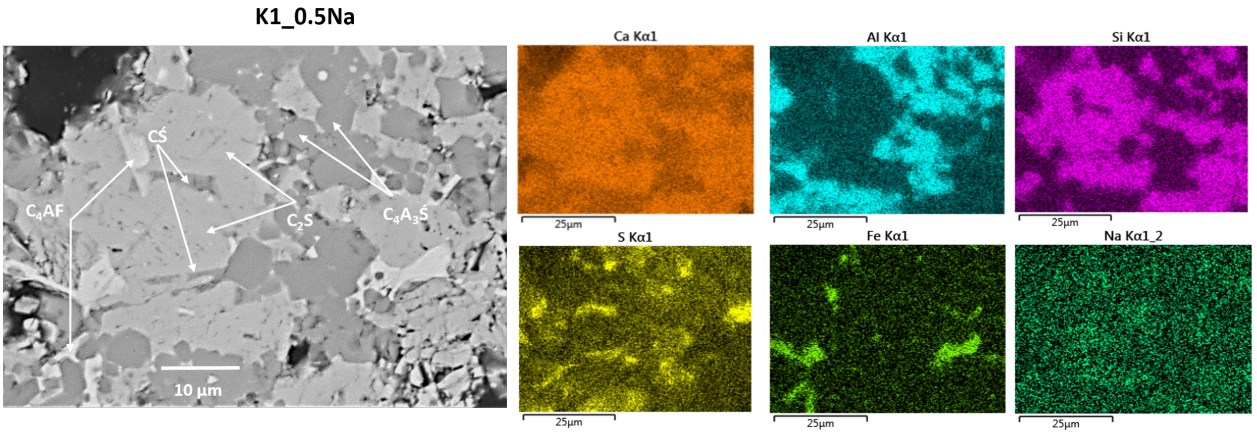

Figure 6. Elemental EDS map for 0.5 Na.

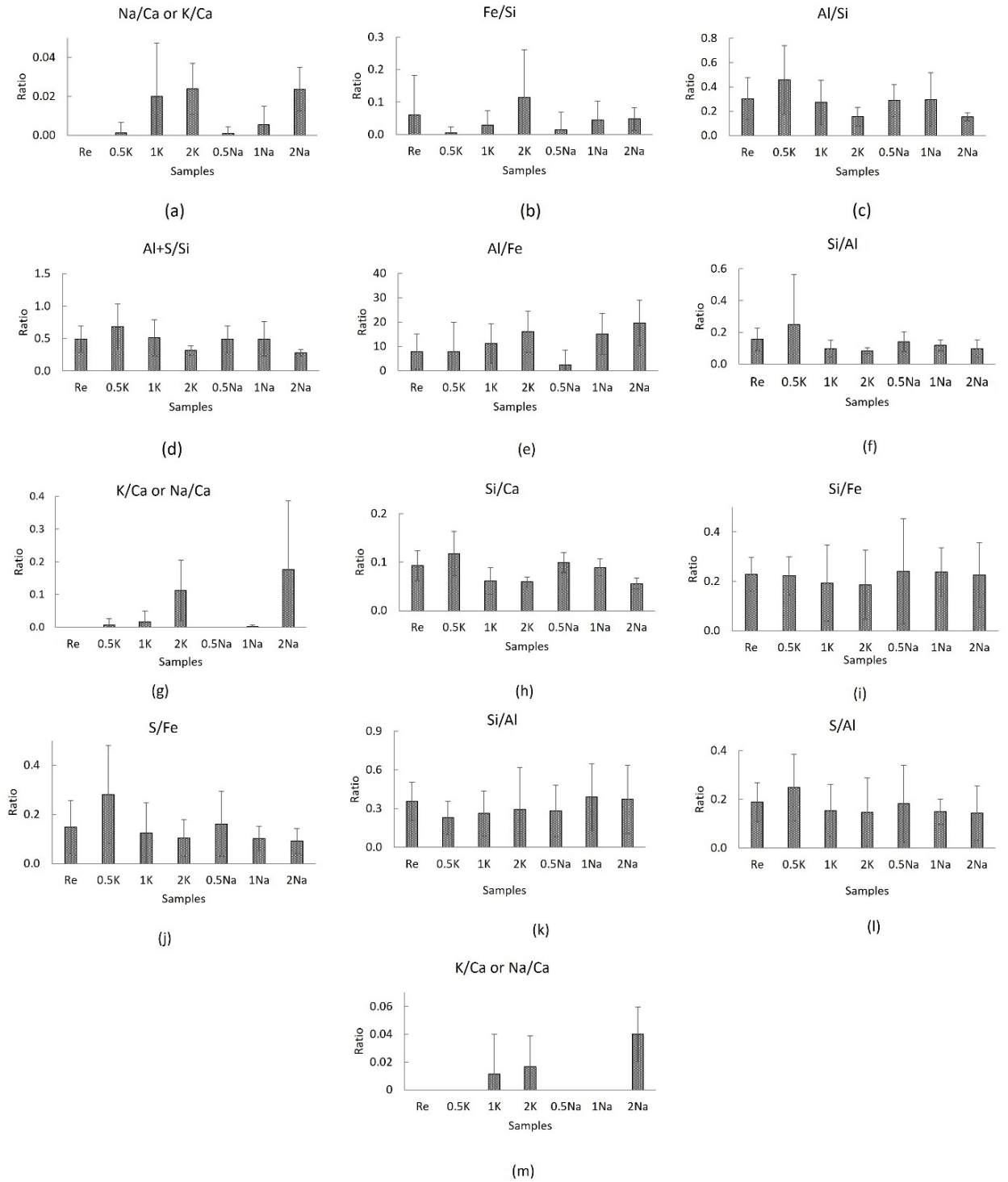

Figure 7. Comparison of the chemical composition of clinker samples, regarding the following clinker phases: belite (a-d), calcium sulfoaluminate (e-h) and ferrite (l-m).

Fe^{3+} is higher in samples with higher alkali content, while the replacement of the same ion by Al^{3+} decreases. With increasing alkali content in the samples, the ratio between the sum of aluminium and sulfur and silicon content generally decreases, which is also reflected in a slight decrease in the d-value of C_2S peaks; Si^{4+} has a lower ratio than Al^{3+} (Table 3). The latter is also the result of the formation of minor components (KŚ, $KC_2Ś_3$, and C_3A) in samples with higher alkali content, where both sulfur and aluminium are consumed [5, 24].

In all studied clinkers, calcium sulfoaluminate included minor elements in the same sequence, with Si and Fe followed by Na or K. It is also interesting to note the Al/Fe ratio (Figure 7e), which affects the shape of the

$C_4A_3\bar{S}$ grains. The higher the alkali content, the larger the Al/Fe ratio in the $C_4A_3\bar{S}$ crystal lattice, indicating higher substitution of Al^{3+} ions by Fe^{3+} ions with larger ionic radii, which was also evidenced by lower d-values of the $C_4A_3\bar{S}$ peaks in samples with a high alkali content (Table 3). The presence of Fe^{3+} in the solid solution leads to the formation of sharper edges of the $C_4A_3\bar{S}$ grains [27] (Figure 5a). In addition to Fe^{3+}, Al^{3+} ions can often be substituted by Si^{4+} (Figure 7f).

Fe^{3+} ions are consumed for C_4AF formation and in C_2S, where they replace Si^{4+} ions. Si^{4+} ions rarely substitute Al^{3+} ions, as they are used to form C_2S. The ratio of potassium or sodium to calcium shows a similar trend (Figure 7g). The more alkalis present in the samples, the greater the substitution of Na^+ or K^+ ions by Ca^{2+} or S^{2-} [4, 26, 33]. Substitution of Ca^{2+} by Na^+ is more pronounced than the replacement of Ca^{2+} by K^+ as a result of haüyn formation [36].

Ion substitution is also observed in the crystal lattice of C_4AF. The Al/Fe ratio, which can be highly variable [40], decreased in proportion to a higher amount of alkalis in the samples (Figure 7h). The latter is consistent with the finding of Gartner et al. [41]. Ca^{2+} can be replaced by alkali cations. Here, we found that the more alkali present in the samples, the greater the substitution of Ca^{2+} ions (Figure 7i). In the samples with a higher alkali content, Al^{3+} ions are often replaced by Si^{4+}, which could be due to the formation of C_3A (Figure 7j). The following ratios S/Ca and S/Al (Figures 7k and 7l) show the same trend – the replacement of the original ions by sulfur decreases in proportion to the increase in the amount of alkali in the samples, which has already been observed as a change in d-values of the C_4AF peaks (Table 3). Namely, sulfur is used to form new phases in the case of the samples with K_2O, and in the case of the samples with the addition of Na_2O, the main reason is the evaporation of SO_3 [24].

Isothermal conduction calorimetry

The heat of hydration of the clinkers is shown in Figure 8. The results show differences for clinkers with alkali addition compared to the reference. Hydration of BCSA cement is a complex process due to the different major and minor phases and is strongly influenced by the amount of gypsum [21, 31]. The major phase of hydration in the early stages is calcium sulfoaluminate, which leads to the formation of ettringite and aluminium hydroxide, while monosulfate forms in the absence of calcium sulphate [42–44]. The first exothermic peak was not completely observed in any of the samples, which can be attributed to the external mixing method. This peak is related to the wetting of the system and rapid dissolution of cement clinker phases [42] and dissolution of soluble alkali sulphates (e.g., $K\bar{S}$ and $KC_2\bar{S}_3$) [45].

As for the samples with K_2O after the initial peak, the sample to which 0.5 wt. % K_2O was added yielded the shortest dormant period followed by two main exothermic peaks. The first occurs after 2 h and the second after 9 h of hydration (Figure 8b). The sample to which 2 wt. % K_2O was added it shows a strong exothermic peak after 3 h of hydration. The main exothermic peaks in the two aforementioned samples are attributed to the dissolution of calcium sulfoaluminate and the formation of ettringite and aluminium hydroxide [31], while the second peak in the 0.5K sample can be attributed to the slow dissolution kinetics of anhydrite [46]. On the other hand, the 1K sample and the samples with Na_2O incorporation reach the first exothermic peak after 50 h for 1K, 40 h for 0.5 and 1Na, and after 75 h for 2Na (Figures 8b and 8c). As can be seen from the total heat evolution curve, the hydration rate slows down after about 40 h. Therefore, the maximum normalized heat flow is 8.0 $mW \cdot g^{-1}$ for the most reactive sample (2K) and 0.5 $mW \cdot g^{-1}$ for the least reactive sample (2Na).

Hydration kinetics depends on the amount of calcium sulfoaluminate as well as other reactive phases such as C_3A, $K\bar{S}$, and $KC_2\bar{S}_3$ [47]. Alkali sulphates were found to accelerate the hydration rate [48]. In addition to $C_4A_3\bar{S}$, C_4AF also accelerate hydration, while the presence of C_2S inhibits it [31, 49]. The 0.5K sample is followed by a reference sample that contains a lot of $C\bar{S}$ compared to other samples, which increases the hydration [24].

In samples with 0.5 or 1 wt. % Na_2O, a high content of $C_4A_3\bar{S}$ was observed, but no C_3A. Additionally, these samples do not contain the alkali sulphates, which have further attenuated the reactivity. The sample with 1 wt. % K_2O contains highly reactive C_3A and alkali sulphates. However, compared to the other two samples with K_2O, it contains the least amount of $C_4A_3\bar{S}$, which weakens its reactivity. The sample with 2 wt. % Na_2O is the least reactive. This sample does not contain alkali sulphates and the amount of $C_4A_3\bar{S}$ and $C\bar{S}$ is the lowest in this sample, while the amount of C_2S is the highest. Here, the amount of Fe^{3+} in C_2S in $C_4A_3\bar{S}$ plays an important role. The larger the amount in these two phases, the slower the hydration [45].

In general, higher cumulative heat is obtained after 7 days for samples with Na_2O (Figure 8f), which was already described in the previous study by Zhao et al. [50]. For both the reference sample and the samples with Na_2O and 1 wt. % K_2O, the cumulative heat first decreases and then increases sharply. In contrast, for the two remaining samples, a significant increase in cumulative heat is observed on the first day of hydration. The evolution of the cumulative heat in the samples coincides with the maximum heat flow released and is related to the amount of major and minor clinker phases, porosity, and Al/Fe ratio in the crystal lattice of the major phases [24, 45]. After 7 days of hydration, the value of cumulative heat in 0.5K and 2K ranged from 84 to 128 $J \cdot g^{-1}$, while it ranged from 176 to 213 $J \cdot g^{-1}$ in the remaining samples (Figures 8e and 8f). The sample with the lowest cumulative heat (2K) has the highest content

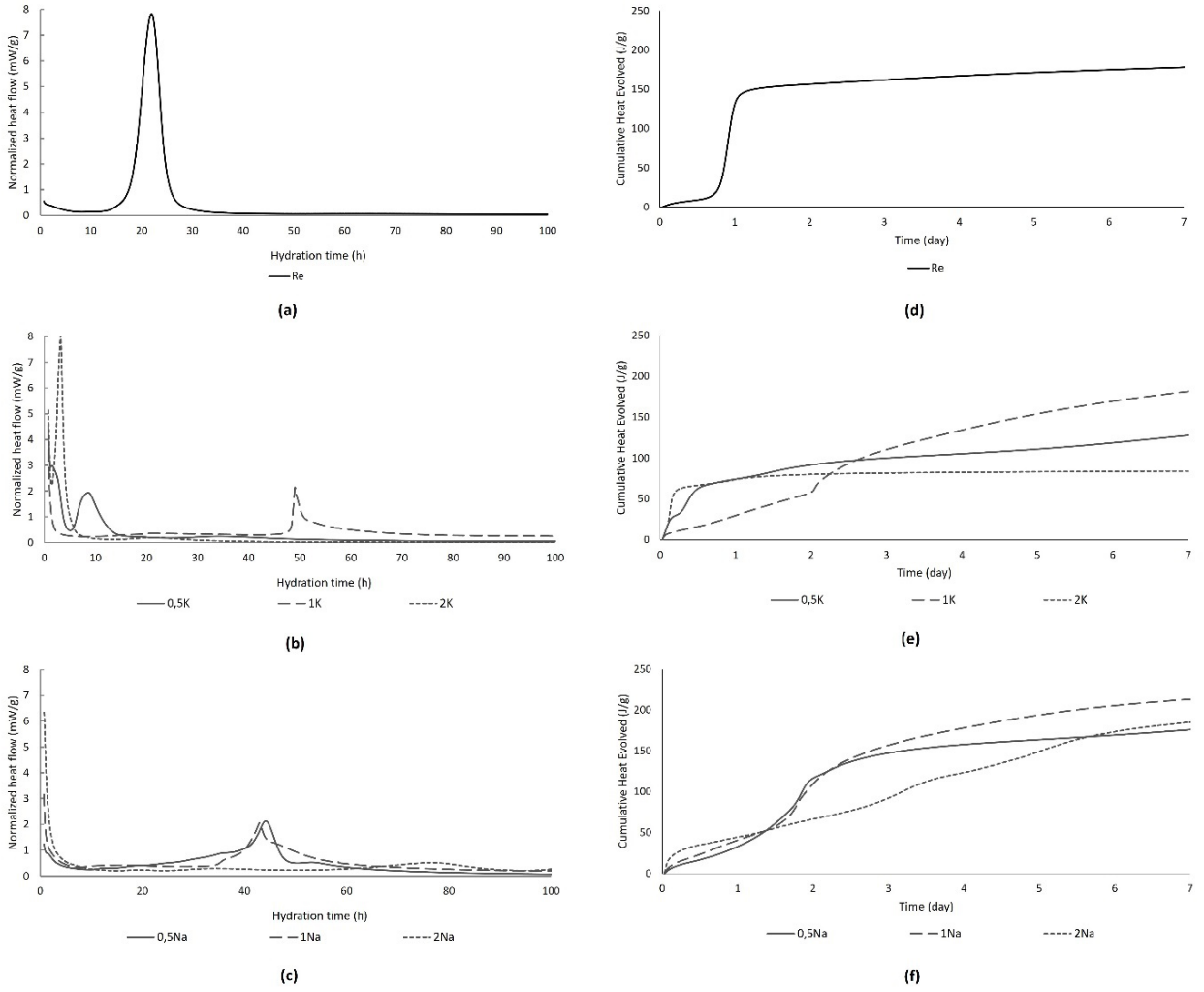

Figure 8. Hydration heat flow for clinker samples: a) Re, b) samples with K_2O, c) samples with Na_2O and cumulative heat for clinker samples d) Re, e) samples with K_2O, f) samples with Na_2O.

of $KC_2\acute{S}_3$ and C_3A, which accelerate the hydration rate. In contrast, the sample with the highest cumulative heat (1Na), has a relatively high content of $C\acute{S}$, a low content of C_3A, and does not contain alkali sulphates that accelerate the hydration rate.

CONCLUSIONS

The paper addresses the effect of alkalis on the microstructure and clinker phase evolution of belite-sulfoaluminate clinker with a target phase composition of 60 wt. % belite, 20 wt. % calcium sulfoaluminate, 10 wt. % ferrite and 10% anhydrite sintered at 1300 °C. In addition to the reference sample, six clinker samples were synthesized with 0.5, 1 and 2 wt. % K_2O and Na_2O, respectively. The reference sample reached the targeted composition, while certain changes in phase compositions were observed in the samples with alkali addition. In general, the amount of C_2S and C_4AF phases increases in samples with higher amount of Na_2O or K_2O, while the amount of $C_4A_3\acute{S}$, and $C\acute{S}$ decreases. The amounts of C_2S, $C_4A_3\acute{S}$, and C_4AF are more variable in samples with Na_2O addition, while they remain approximately the same in samples with K_2O addition. In addition to the major clinker phases, minor phases occurred in samples with alkali addition: C_3A, $K\acute{S}$ and $KC_2\acute{S}_3$.

Foreign ions are also incorporated into the crystal lattice of the major phases. In belite, Ca^{2+} was replaced by Na^+ and K^+, while Si^{4+} was replaced by Al^{3+}, Fe^{3+}, and S^{2-}. In calcium sulfoaluminate, Al^{3+} was replaced by Si^{4+} and Fe^{3+}, while Ca^{2+} was replaced by Na^+ and K^+. In ferrite, Al^{3+} and Fe^{3+} were substituted with Si^{4+} and S^{2-}, while Ca^{2+} was replaced by Na^+ and K^+. The variation in phase composition also affects the shape of the major phase grains in both the reference and alkali-containing samples. In the reference sample, the C_2S grains are mostly spherical, whereas subhedral and anhedral grains predominate in the alkali-incorporated samples. $C_4A_3\acute{S}$ grains are euhedral in the reference samples and hexagonal in low alkali samples, while subhedral and spherical grains predominate in the samples with high

content of both types of alkalis. Regardless of alkali type, C_4AF grains in both the reference and low alkali samples are euhedral and commonly long-prismatic. With increasing alkali content, they become subhedral. The shape of the $C_4A_3\acute{S}$ and C_4AF grains is strongly influenced by the Al/Fe ratio. The increase in Al/Fe ratio in $C_3A_4\acute{S}$ is more pronounced in samples to which Na_2O was added, while in C_4AF the Al/Fe ratios decrease similarly with both types of alkalis, however higher values were observed in samples with K_2O addition.

The variations in phase composition also affect the reactivity of the clinker. Despite the generally high content of calcium sulfoaluminate in the reference sample and the clinkers to which Na_2O was added, these samples were less reactive than the samples to which K_2O was added, indicating the importance of the presence of highly reactive minor phases, e.g., $K\acute{S}$ and $KC_2\acute{S}_3$. The most reactive sample, in which the main exothermic peaks occurred after 3 h, was 2K sample, followed by a reference sample and 0.5K sample. For samples with Na_2O, the main exothermic peaks occurred after 40 h for 0.5Na and 2Na and after 75 h for 2Na.

The study showed that the presence of alkalis affects the phase composition of clinkers and consequently their microstructure (shape of grains). Moreover, the incorporation of Na_2O in mixture decreases the hydration rate, while K_2O, more precisely the formation of the new phases (e.g., alkali sulphates) accelerates it.

Acknowledgment

This research was financial support from the Slovenian Research Agency (research core funding No. P2-0273).

REFERENCES

1. Andrew R.M. (2019): Global CO_2 emissions from cement production, 1928-2018. *Earth Syst Sci Data, 11*, 1675–1710. doi:10.5194/essd-11-1675-2019
2. Gartner E., Sui T. (2018): Alternative cement clinkers. *Cement and Concrete Research, 114*, 27-39. doi:10.1016/j.cemconres.2017.02.002
3. Shi C., Fernández-Jiménez A., Palomo A. (2011): New cements for the 21st. century: the pursuit o fan alternative to portland cement. *Cement and Concrete Research, 41*, 750–763. doi: 10.1016/j.cemconres.2011.03.016
4. Quillin K. (2001): Performance of belite-sulfoaluminate cements. *Cement and Concrete Research, 31*, 1341–1349. doi:10.1016/S0008-8846(01)00543-9
5. Odler I. (2000). *Special inorganic cements.* Taylor&Francis, New York
6. Morsli K., de la Torre Á.G., Zahir M., Aranda M.A.G. (2007): Mineralogical phase analysis of alkali and sulfate bearing belite rich laboratory clinkers. *Cement and Concrete Research, 37*, 639–646. doi:10.1016/j.cemconres.2007.01.012
7. Žibret L., Šter K., Borštnar M., et al. (2021): The incorporation of steel slag into belite-sulfoaluminate cement clinkers. *Applied Science, 11*, 1840. doi:10.3390/app11041840
8. Majling J., Sahu S., Vlna M., Roy D.M. (1993): Relationship between raw mixture and mineralogical composition of sulphoaluminate belite clinkers in the system $CaOSiO_2Al_2O_3Fe_2O_3$ SO_3. *Cement and Concrete Research, 23*, 1351–1356. doi:10.1016/0008-8846(93)90072-H
9. Kolovos K., Tsivilis S., Kakali G. (2005): SEM examination of clinkers containing foreign elements. *Cement and Concrete Composites, 27*, 163–170. doi:10.1016/j.cemconcomp.2004.02.003
10. Odigure J.O. (1996): Mineral composition and microstructure of clinker from raw mix containing metallic particles. *Cement and Concrete Research, 26*, 1171–1178. doi:10.1016/0008-8846(96)00111-1
11. Long G.R. (1983): Microstructure and Chemistry of Unhydrated Cements. *Philosophical Transactions of the Royal Society of London. Series A, Mathematical and Physical Sciences, 310*, 43–51. doi:10.1098/rsta.1983.0064
12. Jawed I., Skalny J.. (1978): Alkalies in cement: A review. *Cement and Concrete Research, 8*, 37–51. doi:10.1016/0008-8846(78)90056-x
13. Zhang J., Gong C., Lu L., et al. (2015): Effect of MgO on the composition and properties of belite-barium calcium sulphoaluminate cement in the presence of Na_2O and K_2O. *Ceramics - Silikaty, 59*, 135–144
14. Ma B., Li X., Mao Y., Shen X. (2013): Synthesis and characterization of high belite sulfoaluminate cement through rich alumina fly ash and desulfurization gypsum. *Ceramics - Silikaty, 57*, 7–13
15. Segata M., Marinoni N., Galimberti M., et al. (2019): The effects of MgO, Na_2O and SO_3 on industrial clinkering process: phase composition, polymorphism, microstructure and hydration, using a multidisciplinary approach. *Materials Characterization, 155,* 1–13. doi:10.1016/j.matchar.2019.109809
16. Shen Y., Qian J., Huang Y., Yang D. (2015): Synthesis of belite sulfoaluminate-ternesite cements with phosphoqypsum. *Cement and Concrete Composites, 63*, 67–75. doi:10.1016/j.cemconcomp.2015.09.003
17. Bouzidi M.A., Tahakourt A., Bouzidi N., Merabet D. (2014): Synthesis and Characterization of Belite Cement with High Hydraulic Reactivity and Low Environmental Impact. *Arabian Journal for Science and Engineering, 39*, 8659–8668. doi:10.1007/s13369-014-1471-2
18. Gotti E., Marchi M., Costa U. (2007): Influence of Alkalis and Sulphates on the Mineralogical Composition of Clinker. In: *12th International Congress on the Chemistry of Cement.* Montréal.
19. Liu X., Liu T., Wu Y., et al. (2013): Effect of alkalis on the mineral formation and properties of alite-sulfoaluminate cement. *Advances in Cement Research, 25*, 98–103. doi:10.1680/adcr.11.00050
20. Kacimi L., Simon-Masseron A., Salem S., et al. (2009): Synthesis of belite cement clinker of high hydraulic reactivity. *Cement and Concrete Research, 39*, 559–565. doi:10.1016/j.cemconres.2009.02.004
21. Morsli K., De La Torre Á.G., Stöber S., et al. (2007): Quantitative phase analysis of laboratory-active belite clinkers by synchrotron powder diffraction. *Journal of the American Ceramic Society, 90*, 3205–3212. doi:10.1111/

j.1551-2916.2007.01870.x
22. Odler I., Wonnemann R. (1983): Effect of alkalies on portland cement hydration I. Alkali oxides incorporated into the crystalline lattice of clinker minerals. *Cement and Concrete Research, 13*, 477–482. doi: 10.1016/0008-8846(83)90005-4
23. Gies A., Knöfel D. (1986): Influence of alkalies on the composition of belite-rich cement clinkers and the technological properties of the resulting cements. *Cement and Concrete Research, 16*, 411–422. doi:10.1016/0008-8846(86)90117-1
24. Bullerjahn F. (2018). *Characterisation and hydration of ye`elimite containing cements*: Ph.D. Dissertation. EPF Lozana, 247 pp.
25. Dolenec S., Šter K., Borštnar M., et al. (2020): Effect of the cooling regime on the mineralogy and reactivity of belite-sulfoaluminate clinkers. *Minerals, 10,* 1–16. doi:10.3390/min10100910
26. Strigáč J., Palou M.T., Krištín J., Majling J. (2000): Morphology and chemical composition of minerals inside the phase assemblage C-C_2S-$C_4A_3\bar{S}$-C_4AF-$C\bar{S}$ relevant to sulphoaluminate belite cements. *Ceramics - Silikaty, 44*, 26–34
27. Touzo B., Scrivener K.L., Glasser F.P. (2013): Phase compositions and equilibria in the CaO-Al_2O 3-Fe_2O_3-SO_3 system, for assemblages containing ye'elimite and ferrite $Ca_2(Al,Fe)O_5$. *Cement and Concrete Research, 54*, 77–86. doi:10.1016/j.cemconres.2013.08.005
28. Žibret L., Ipavec A., Dolenec S. (2022): Microstructural characteristics of belite–sulfoaluminate cement clinkers with bottom ash. *Construction and Building Materials, 321*, 126289. doi:10.1016/j.conbuildmat.2021.126289
29. Andac O., Glasser F.P. (1995): Microstructure and microchemistry of calcium sulfoaluminate cement. *Mater Res Soc Symp - Proc, 370*, 135–142. doi:10.1557/proc-370-143
30. Duda W.H. (1985). *Cement Data Book*, Volume One: International Process Engineering in the Cement Industry, 3rd ed. French & European Publications, Berlin
31. Chen I.A., Juenger M.C.G. (2011): Synthesis and hydration of calcium sulfoaluminate-belite cements with varied phase compositions. *Journal of Materials Science, 46*, 2568–2577. doi:10.1007/s10853-010-5109-9
32. Herfort D., Moir G.K., Johansen V., et al. (2010): The chemistry of Portland cement clinker. *Advances in Cement Research, 22*, 187–194. doi:10.1680/adcr.2010.22.4.187
33. Cuesta A., De La Torre Á.G., Losilla E.R., et al. (2014): Pseudocubic crystal structure and phase transition in doped ye'elimite. *Crystal Growth and Design, 14*, 5158–5163. doi:10.1021/cg501290q
34. Xiuji F., Shizong L. (1986): Investigation of the effect of minor ions on the stability of β-C_2S and the mechanism of stabilization. *Cement and Concrete Research, 16*, 587–601. doi:10.1016/0008-8846(86)90097-9
35. Koumpouri D., Karatasios I., Psycharis V., et al. (2021): Effect of clinkering conditions on phase evolution and microstructure of Belite Calcium-Sulpho-Aluminate cement clinker. *Cement and Concrete Research, 147*, 106529. doi:10.1016/j.cemconres.2021.106529
36. Hargis C.W., Telesca A., Monterio P.J.M. (2014): Calcium sulfoaluminate (ye`elimite) hydration in the presence of gypsum, calcite and vaterite. *Cement and Concrete Research, 65*, 15–20. doi:10.1016/j.cemconres.2014.07.004
37. Zhu J., Chen Y., Zhang L., et al. (2020): Insights on substitution preference of Pb ions in sulfoaluminate cement clinker phases. *Materials (Basel), 14*, 44. doi:10.3390/ma14010044
38. Saidani S., Smith A., El Hafiane Y., Ben Tahar L. (2021): Role of dopants (B, P and S) on the stabilization of β-Ca_2SiO_4. *Journal of the European Ceramic Society, 41*, 880–891. doi:10.1016/j.jeurceramsoc.2020.07.037
39. Lai G.C., Nojiri T., Nakano K. (1992): Studies of the stability of β-Ca_2SiO_4 doped by minor ions. *Cement and Concrete Research, 22*, 743–754. doi:10.1016/0008-8846(92)90097-F
40. Ben Haha M., Winnefeld F., Pisch A. (2019): Advances in understanding yeelimite rich cements. *Cement and Concrete Research, 123*, 105778. doi: 10.1016/j.cemconres.2019.105778
41. Gartner E.M., Young J.F., Damidot D.A., Jawed I. (2002): Hydration of portland cement. In: Bensted J., Barnes P. (eds): *Structure and performance of cements*. Taylor and Francis, New York, pp. 83–84
42. Borštnar M., Daneu N., Dolenec S. (2020): Phase development and hydration kinetics of belite-calcium sulfoaluminate cements at different curing temperatures. *Ceramics International, 46*, 29421–29428. doi:10.1016/j.ceramint.2020.05.029
43. Cuberos A.J.M., De La Torre Á.G., Álvarez-Pinazo G., et al. (2010): Active iron-rich belite sulfoaluminate cements: Clinkering and hydration. *Environmental Science & Technology, 44*, 6855–6862. doi:10.1021/es101785n
44. Mrak M., Winnefeld F., Lothenbach B., Dolenec S. (2021): The influence of calcium sulfate content on the hydration of belite-calcium sulfoaluminate cements with different clinker phase compositions. *Materials and Structures, 54*, 212. doi:10.1617/s11527-021-01811-w
45. Bullerjahn F., Ben Haha M., Scrivener K.L. (2015): Iron solid solutions of yeelimite – effect on reactivity. In: *14th International Congress on the Chemistry of Cement.* Beijing, pp. 1–15
46. Winnefeld F., Martin L.H.J, Müller C.J., Lothenbach B. (2017): Using gypsum to control hydration kinetics of CSA cements. *Construction and Building Materials, 155*, 154–163. doi:10.1016/j.conbuildmat.2017.07.217
47. Ghoroi C., Suresh A.K. (2007): Solid-solid reaction kinetics: Formation of tricalcium aluminate. *AIChE Journal, 53*, 502–513. doi:10.1002/aic.11086
48. Lee J.K., Chu Y.S., Kwon C.W. (2007): The effects of alkali sulfate on the hydration of a C_3A- $CaSO_4 \cdot 2H_2O$ system. *Journal of the Korean Ceramic Society, 44*, 471–476. doi:10.4191/KCERS.2007.44.9.471
49. Sharp J.H., Lawrence C.D., Yang R. (1999): Calcium sulfoaluminate cements - Low-energy cements, special cements or what? *Advances in Cement Research, 11*, 3–13. doi:10.1680/adcr.1999.11.1.3
50. Zhao Y., Lu L., Wang S., et al. (2015): Dicalcium silicates doped with strontia, sodium oxide and potassia. *Advances in Cement Research, 27*,311–320. doi:10.1680/adcr.14.00011